Emergence of alternative stable states in gene exchange communities

Juken Hong[1], Wenzhi Xue[1], Teng Wang[1]✉

[1]Key Laboratory of Quantitative Synthetic Biology, Shenzhen Institute of Synthetic Biology, Shenzhen Institutes of Advanced Technology, Chinese Academy of Sciences, Shenzhen 518055, China.

✉Corresponding author. Email: t.wang1@siat.ac.cn.

Abstract

Microbial communities living in the same environment often display multiple alternative stable states, each characterized by a unique composition of species. Understanding the origin and determinants of microbiome multistability has broad implications in environments, human health and microbiome engineering. However, despite its conceptual importance, how multistability emerges in complex communities remains largely unknown. Here, we focused on the role of horizontal gene transfer (HGT), one important aspect mostly overlooked in previous theories, on the stability landscape of competing microbial populations. Combining theoretical derivation and numerical simulations, we demonstrated that in many scenarios increasing gene transfer rate could promote the emergence of many alternative stable states in complex microbiota. In metacommunities composed of multiple local patches, such multistability enabled by HGT allows the regional coexistence of diverse microbes which would otherwise outcompete each other. We further discussed the effects of different complicating factors on the role of HGT in mediating microbiome stability. Our results provide key insights for the predictive control and engineering of complex microbiota.

Introduction

Microbial communities living in similar environments often display different community types, each characterized by a unique composition of species[1-4]. Changes in environmental factors, fluctuations of species abundances, or transient invasions can trigger abrupt and irreversible transitions between two types[5-7]. Such transitions, also known as regime shifts, lead to the dramatic alterations of microbiome functions and are tightly associated with many host diseases, soil fertility, marine biogeochemical flux, or bioproduction yield[8-12]. Understanding the origin of different community types has broad implications in environments, engineering and health[1,3].

Multistability, a phenomenon where multiple stable states coexist for the same set of system parameters, is one of the most important mechanisms behind alternative community types and has been widely observed in a variety of natural or experimental microbiomes[1,4,7,13-17]. Under perturbations, a multistable system can be driven away from a former stable state, cross the tipping point and reach a new steady state. The population can persist in the new state even after the perturbations are withdrawn, exhibiting a behavior of 'hysteresis'[3,13]. Despite its conceptual importance, the determinants underlying microbiota multistability have been poorly understood due to the intrinsic complexity of microbial interactions[14].

Unraveling how multistability emerges in complex microbiota can provide crucial insights in different scenarios. For instance, the existence of alternative 'hidden' stable states in gut microbiome undermines the community resilience against external perturbations such as pathogenic infections or dietary changes[18]. Understanding which mechanisms contribute to multistability will help the design of modulatory strategies that prevent the developments of unhealthy stable states[8,18]. Multistability also renders the catastrophic shift of microbial populations under antibiotic exposure from being drug-sensitive to drug-resistant[6]. Inhibiting the processes underlying multistability can be useful to reverse antibiotic resistance and prolong the efficacy of current antibiotics[19]. In engineered microbiomes, the drastic compositional changes can result in the unexpected loss of the desired functions. The ability to predict and control community

multistability is essential to better harness the bioproduction potential of synthetic microbial consortia[15].

Mathematical models are indispensable to decipher the emergent properties of complex populations[20]. While different ecological models have been developed to analyze the influences of some factors, such as microbial mutual inhibition and nutrient stoichiometries, in mediating community multistability, the roles of many critical mechanisms have been overlooked in existing theories[1,14]. Chief among these is horizontal gene transfer (HGT), a process where microbes share mobile genetic elements (MGEs) with their neighbors[21]. Indeed, HGT is prevalent in microbial world and mobile genes occupy a substantial proportion in microbial gene pool[22-24]. For instance, among the closely related microbial isolates in the same human body site, HGT occurs in more than 40% of the species pairs[25]. In the draft genomes of human gut microbes, tens of thousands of genes were mobilizable[23]. However, despite its functional and ecological importance, the interplay between genetic exchange and community multistability has not been rigorously examined in previous studies and a general conclusion remains lacking.

In this work, we focus on communities of competing microbes, a model system for microbiome multistability[1,14,26]. By combining theoretical analysis and numerical simulations, we demonstrated that in many scenarios gene transfer could promote the emergence of alternative stable states which otherwise would not exist. We further extended our analysis to metacommunities consisting of multiple local habitats. Our results suggested that while multistability enabled by HGT didn't affect local diversity, it enabled the emergence of species diversity at regional scale. We also discussed the influence of different confounding factors on the applicability of the predictions. Our results provide valuable insights for microbial ecology, health and microbiome engineering.

Results

The role of HGT on bistability of two-species populations

To illustrate the basic concepts, let's first consider a population of two competing species. The mutual inhibition between the two members creates a positive feedback, making bistability possible[1,14]. Without HGT, the community dynamics can be simulated by the classic Lotka-Volterra (LV) model that accounts for species growth rates (μ_1 and μ_2), interspecies competition (γ_1 and γ_2) and the dilution rate (D). Given the simplicity of this model, the condition of the system being bistable can be analytically solved as $\gamma_1 > \phi_2/\phi_1$ and $\gamma_2 > \phi_1/\phi_2$ where $\phi_1 = \frac{\mu_1 - D}{\mu_1}$ and $\phi_2 = \frac{\mu_2 - D}{\mu_2}$ (see Methods for more details). When this condition is satisfied, either species can dominate the population at steady state, depending on their initial abundances. Otherwise, the population will always rest at the same steady state regardless of the initial composition (Fig. 1a).

To analyze the effect of HGT on bistability, we applied a mathematical model that we previously developed to describe gene transfer between competing species[27]. Compared with the classic LV model, the new framework considered the growth rate of each species as a combination of two components contributed by non-mobilizable genes and mobile genes, respectively (see Methods for more details). Due to the fitness effects of mobile genes (denoted as λ_1 and λ_2, respectively), their gain and loss within each species caused the dynamic change of species growth rates. Gene transfer (with the rate denoted as η) allows the two competitors to partially exchange their fitness benefits or disadvantages, and we sought to understand whether this process would reshape the stability landscape of the system.

Due to the increase of modeling complexity, analytical solution becomes infeasible for the new framework. Instead, we determined whether the system was bistable by numerical simulations with randomized initial compositions[26]. In general, the resolution of this approach increases with the number of randomizations. Without loss of generality, here we randomly initialized the species abundances for 200 times between 0 and 1 following uniform distributions (Fig. S1a). Then we simulated the population dynamics for each initialization until steady state and obtained their species abundances. A system is called monostable if all populations starting from different compositions converge into the same state. In contrast, if two attractors exist, the system is called

bistable (Fig. 1a). We calculated the number of stable states for a wide range of μ_1 and μ_2 values and drew the phase diagram (Fig. 1b). Whether it is easy for the system to achieve bistability is reflected by the total area of bistability region on the phase diagram. Our numerical results suggested that increasing HGT enlarged the region, creating bistability in a lot of systems which would otherwise be monostable (Fig. 1b-d). Here, the number of initializations was not critical for the conclusion (Fig. S1a). The results also hold for populations with a variety of interspecies competitions or gene transfer rates (Fig. S1b-d), suggesting the robustness of our conclusion against a variety of confounding factors.

Our results suggested that increasing HGT made it more feasible for the system to become bistable. However, this should not be taken as an assertion that the system will always be bistable when HGT exists (Fig. 1c and d). The effect of HGT in creating bistability in a specific community depends on the competition strength, gene transfer rate and the fitness difference between species (Fig. 1b-d). Bistability will not appear when $\gamma_1\gamma_2 < 1$, regardless of HGT rate (Methods). In addition, for two species with large fitness difference, the system might remain monostable when gene transfer rate increases (Fig. 1c). In this case, the strong competitor will always win despite the gene flow. The effect of HGT in promoting bistability is more applicable between species with smaller fitness difference and stronger competition (Fig. 1b-d, Fig. S1b).

HGT shapes the stability landscape of multi-species communities

The modeling framework can be readily generalized to more complex communities consisting of multiple competing species by taking into account the gene transfer between every pair of species (see Methods for more details). To understand how gene transfer rate affects the stability landscape of complex microbiota, we estimated the number of alternative stable states by randomly initializing the abundance of each species 500 times between 0 and 1 following uniform distributions. For each initialization, we simulated the population dynamics for 2000 hours till the systems reached equilibrium and calculated the steady-state abundances of different species (Fig. S2). Limit cycles were not observed in our simulations (Fig. S3).

The stability landscape of a complex community can be characterized by the absolute number of stable states. To this end, we grouped the steady states into different attractors using a given threshold. Two steady states with their Euclidean distance smaller than the threshold belonged to the same group (Fig. S4). However, the estimation of this number can be biased by the intrinsic limitations of the numerical approach. For instance, the limited number of initializations can underestimate this number. In contrast, the inability of a system to reach equilibrium within the limited time window of simulations can cause its overestimation. To overcome such limitations, we developed an alternative metric χ to measure the multistability of a system by borrowing the concept of 'entropy'. Let φ be the number of stable states and x_i be the relative size of each domain of attraction ($\sum_i x_i = 1,\ i = 1,2,\dots,\varphi$). χ is calculated as $\chi = exp\,(-\sum_i x_i log x_i)$, which accounts for the absolute number of stable states as well as the size of each basin. χ equals 1 in monostable systems. χ gets larger when more stable states emerge or the distribution of the basin sizes become more even. Numerical tests suggested that χ was robust to the variations of distance threshold, simulation timespan or number of initializations (Fig. S5).

As shown in Fig. 2, when HGT is absent, the number of stable states is usually small in a multi-species population. Increasing gene transfer rate reshaped the stability landscape of a microbiome by creating additional stable states. Each stable state is characterized by a different dominant species (Fig. 2a). This prediction is generally applicable to communities consisting of different number of species (Fig. S6).

So far, our analysis has been focused on communities where the interaction network is fully connected, and each species competes with every other member. In each of such populations, it is highly infeasible to achieve the stable coexistence of different species. While this analysis provides the basic proof of principle, natural environments often consist of many niches[28]. Species living in the same niche compete with each other while species from different niches can coexist. To understand whether our conclusion is still applicable when niche effects are considered, we extended our analysis to communities carrying a random number of niches. Each species was randomly allocated into one of the niches, and the stability landscape was analyzed in the same

way by randomly initializing the systems (see Methods for more details). Our results suggest that increasing HGT rate still promotes multistability, regardless of the niche structure of the competing communities (Fig. 3).

HGT-enabled multistability promotes the regional coexistence of competing species

Our results highlight the role of HGT on shaping the stability landscape of closed local communities. Natural microbiomes, however, exist at scales broader than a localized population. A set of local communities subject to similar environments, also known as 'patches', form a metacommunity[29,30]. When multiple stable states coexist, the compositions of different patches may differ from each other due to the variability of their initial species occupation. Collectively, the multistability in the local patches might give rise to the regional species diversity in the metacommunity. This intuition leads to our hypothesis that HGT allows the stable coexistence of multiple competing species at regional scale, even when species exclusively outcompete each other in every local population.

To examine this hypothesis, we constructed metacommunities of 100 patches connected by dispersal of microbes. Without loss of generality, we considered a 2-D array of local patches and assumed that the dispersal only occurred between adjacent patches (Fig. 4a, see Methods for more details). Each local patch carried 10 competing species that exchanged mobile genes with each other. The dynamics of each patch was governed by the same set of parameters but initialized with different species compositions. We then numerically simulated the dynamics of the metacommunity till it reached steady state.

Without HGT, the metacommunity exhibited strong spatial homogeneity at regional scale (Fig. 4b). Different patches rested at similar species compositions. In contrast, HGT created a spatial pattern of species distributions across different patches, due to the emergent multistability (Fig. 4b). To analyze the influence of HGT on regional diversity, we pooled all local populations together and calculated the collective species diversity in the pool using Shannon index. Our results suggested that while local diversity remained low regardless of HGT rate, the regional diversity of

microbial species increased with HGT rate (Fig. 4b and c). The conclusion is applicable for different dispersal rates (Figs. S7 and S8). These results highlight the fundamental role of HGT in community stability and diversity at local and regional scale.

The influences of different confounding factors on the role of HGT in mediating population multistability

Our previous analysis has focused on the role HGT in communities where: (1) MGEs only affect species growth rates and have no influences on inter-species competition; (2) the fitness effects of MGEs (λ_1 and λ_2) are independent of the host species. To understand how these assumptions affected the prediction and clarify the potential caveats of our conclusion, we further extended our modeling framework by accounting for different confounding factors.

In nature, the horizontal transfer of some genes can change the competition strengths between different species. For instance, the sharing of many mobile genes can promote niche overlapping, leading to an increase of competition strength[31,32]. Some mobile genes encode public goods that benefit the host's neighboring species[33,34]. HGT of these genes will reduce the strength of interspecies competition. To understand how the transfer of these genes would influence community bistability, we adapted the previous model by considering the dynamic change of competition strength during HGT (see Supplementary Materials for more details). In particular, for two-species populations, we divided the interspecies competitions into two components: the basal competition strengths (γ_1 and γ_2) and the added parts by HGT (δ_1 and δ_2). The overall competition strength was calculated as $\gamma_1 + \delta_1 \frac{p_1}{s_1}$ and $\gamma_2 + \delta_2 \frac{p_2}{s_2}$, respectively. Positive δ's mean HGT promotes the inter-species competition, while negative δ's mean HGT reduces competition. Numerical simulations with randomized parameters suggested that when δ's were positive, HGT still promoted the bistability, whereas if δ's were negative, gene transfer would reduce the chance of bistability (Fig. 5a-d). We further extended our analysis to multispecies communities and calculated the number of stable states. As shown in Fig. 5e and f, the number of

stable states increases with HGT rate when MGEs promotes competition, while decreases with HGT rate when MGEs reduces competition.

In previous analysis, we also assumed that the effects of MGEs on host growth (λ_1 and λ_2) were independent of the host species. In nature, however, the same MGE can have different fitness effects in different genomic backgrounds, a phenomenon called epistasis[35-38]. There are two types of epistasis: magnitude epistasis, where the host genomic background only affects the magnitude but not the sign of λ value, and sign epistasis, where the same MGE is burdensome in one species while beneficial in the other host. The model can be readily extended to account for these two types of epistasis (see Supplementary Materials for more details). In particular, we dissected the growth rates μ_1 and μ_2 into two components: the basal growth rate (μ_1^0 and μ_2^0), and the fitness effects (λ_{11} and λ_{22}) of the mobilizable genes. The growth rates of p_1 and p_2 were calculated as $\mu_1(1+\lambda_{12})$ and $\mu_2(1+\lambda_{21})$, respectively. Here λ_{ij} $(i,j=1,2)$ stands for the fitness effects of the j-th mobile gene in the i-th species. Without epistasis, the fitness effects are independent of the host species ($\lambda_{11}=\lambda_{21}$ and $\lambda_{22}=\lambda_{12}$). The epistasis can be quantified by two ratios: $\xi_1=\lambda_{21}/\lambda_{11}$ and $\xi_2=\lambda_{12}/\lambda_{22}$. $\xi_1>0$ and $\xi_2>0$ represent magnitude epistasis, whereas $\xi_1<0$ or $\xi_2<0$ represent the sign epistasis. We carried out additional numerical simulations to evaluate how different epistasis types influence the role of HGT in community stability. Our results suggested that with magnitude epistasis, HGT still enlarged the area of bistability region (Fig. 6a and b). In contrast, sign epistasis overturned HGT's role on community stability: with sign epistasis, increasing gene transfer rate reduced the area of bistability region (Fig. 6c and d). These results suggest that MGE epistasis might add another layer of complexities into the interplay between HGT and community stability.

The fitness effect of an MGE can be extreme in some cases. For instance, under strong antibiotic selection, only cells carrying the antibiotic resistant genes (ARGs) can survive. To examine whether our conclusion is still applicable in this scenario, we generalized our model by considering the transfer of an ARG in a population under strong antibiotic selection (see Supplementary Materials for more details). Specifically, we assumed that the ARG was initially

234 carried by one species in the populations. Without HGT, only the donor species carrying the ARG
235 can survive due to antibiotic selection (Fig. 7a). In this case, the system will always be monostable
236 regardless of the initial species compositions. With HGT, the ARGs can be transferred to other
237 species, creating chances for other species to survive (Fig. 7b). To understand how HGT affects
238 community stability under this condition, we first analyzed the phase diagram of the two-species
239 population. Our simulation results suggested that bistability became possible when there existed
240 gene transfer and increasing HGT rate in general enlarged the bistability area (Fig. 7c and d). Here,
241 without loss of generality we assumed that the ARG was initially carried only by species 1.
242 Bistability was more feasible when $\mu_2 > \mu_1$ (Fig. 7c), suggesting that the effect of HGT on
243 promoting bistability will be stronger when the weak competitor acts as the ARG donor. We further
244 analyzed the number of stable states in complex communities transferring an ARG. As shown in
245 Fig. 7e and f, for these populations under antibiotic selection, increasing transfer rate of the ARG
246 also promoted the emergence of multistability, suggesting the general applicability of our
247 prediction in this scenario.

248 **Discussion**

249 Our work predicts that in many scenarios horizontal gene flow promotes multistability in
250 communities of competing microbes. At the scale of local populations, the emergence of
251 alternative stable states undermines the global stability of the community, making the system less
252 resilient to perturbations on species abundances and creating greater opportunities for regime shifts.
253 In metacommunities, gene flow creates spatial heterogeneity of species compositions in different
254 patches. Despite the low diversity in every local patch, HGT-driven multistability creates
255 substantial diversity at regional scale. In microbial ecology, how microbes competing for a limited
256 number of resources stably coexist has been a long-standing puzzle[39,40]. Our results highlight the
257 importance of considering gene exchange when addressing this fundamental challenge.

258 While this work predicts the potential role of HGT in microbiota diversity and stability, several
259 caveats need to be considered when applying this prediction. For MGEs with sign epistasis, or

MGEs that relax interspecies competitions, HGT might reduce the number of stable states. The relative importance of gene flow in a real community might also be context dependent. The effect of HGT in promoting multistability might be stronger between species with intense competition and similar fitness. In environments with high cell density and abundant MGEs, such as mammal gut, the role of HGT will also be more prominent[41]. In contrast, the influence of HGT on community multistability might become less important in populations with poor cell density and slow gene transfer. Nevertheless, by comparison with empirical estimates of plasmid conjugation rates from a previous study[42], the HGT rates in our analysis are biologically relevant in a variety of natural environments (Methods).

Previous studies documented the presence of multiple alternative community types in soil[15], human vaginal, gut and oral microbiomes[2,43,44]. In particular, multiple groups of bacteria in human gut exhibit robust bistable abundance distributions, resulting in over 32 different stable state combinations[45]. Our results provide a plausible explanation for the large number of community types in these populations, even though our interpretation doesn't exclude other mechanisms including gradients of environmental factors[1]. Disentangling the contributions of HGT from the other factors in diverse natural microbiomes is a promising topic for future research.

Controlling the multistability of complex microbiota has important applications in human health. For instance, in gut microbiome, the development of unhealthy stable states is closely related to many diseases such as obesity, type 2 diabetes mellitus and gastrointestinal disorders[46-48]. Strategies have been developed to overcome the resilience of unhealthy states, including fecal transplantation or supplementation with probiotics[18]. Our work predicts that the horizontal transfer of MGEs such as plasmids might be an additional mechanism for the emergence of the unhealthy states. Indeed, human gut is a 'hotspot' of gene flow[41]. Therefore, inhibiting the MGE spread using small molecules might offer new opportunities to reshape the stability landscape and narrow down the attraction domains of the disease states[49,50].

Figures

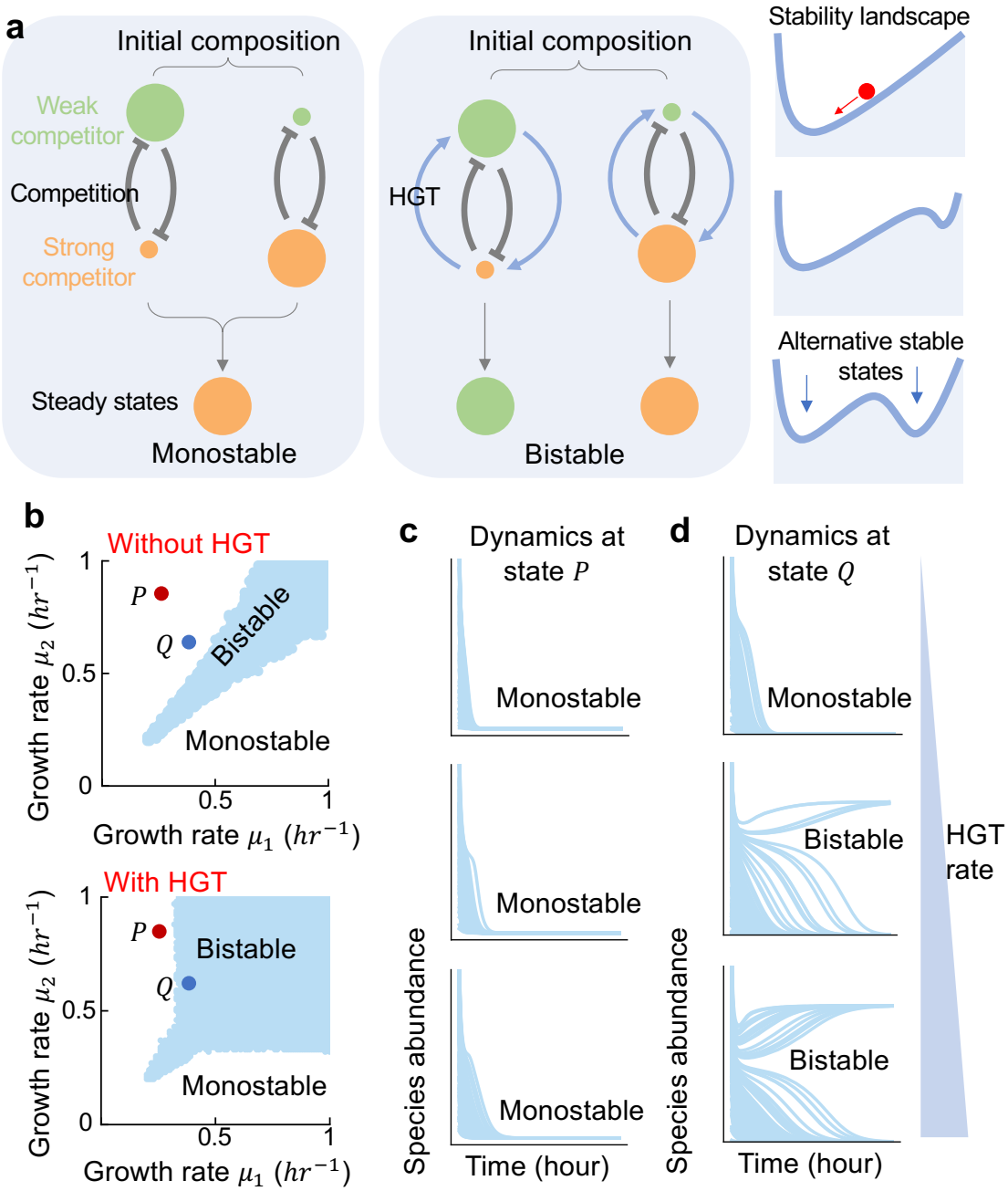

Fig. 1| Horizontal gene transfer (HGT) promotes bistability of communities consisting of two competing microbes.

(a) Schematics of monostable and bistable systems. A monostable system will always rest at the same steady state no matter where the system starts from. In contrast, a bistable system can reach two distinct steady states, depending on the initial ratio between the two competitors.

(b) The phase diagram of the population with (bottom panel, $\eta = 0.2\ hr^{-1}$) or without HGT (top panel). Different combinations of μ_1 and μ_2 between 0 and 1 hr^{-1} were tested. For each combination, the initial abundance of each species was randomized 200 times between 0 and 1 following uniform distribution. The system was monostable if all initializations led to the same steady state. Otherwise, the system was bistable. All combinations of μ_1 and μ_2 that led to bistability were marked in blue in the diagram. Other parameters are $\gamma = 1.1$, $\kappa = 0.005\ hr^{-1}$, $D = 0.2\ hr^{-1}$, $\mu_1^0 = \mu_2^0 = 0.5\ hr^{-1}$. Two states, P ($\mu_1 = 0.3\ hr^{-1}$, $\mu_2 = 0.8\ hr^{-1}$) and Q ($\mu_1 = 0.4\ hr^{-1}$, $\mu_2 = 0.6\ hr^{-1}$), were labeled as examples.

(c-d) Population dynamics of P and Q under 100 different initializations. Here, the dynamic changes of species 1's abundance were shown. Three different HGT rates (0, 0.1, 0.2 hr^{-1} from top to bottom) were tested. When gene transfer rate increases, the system at Q changed from monostable to bistable, while the system at P remained monostable.

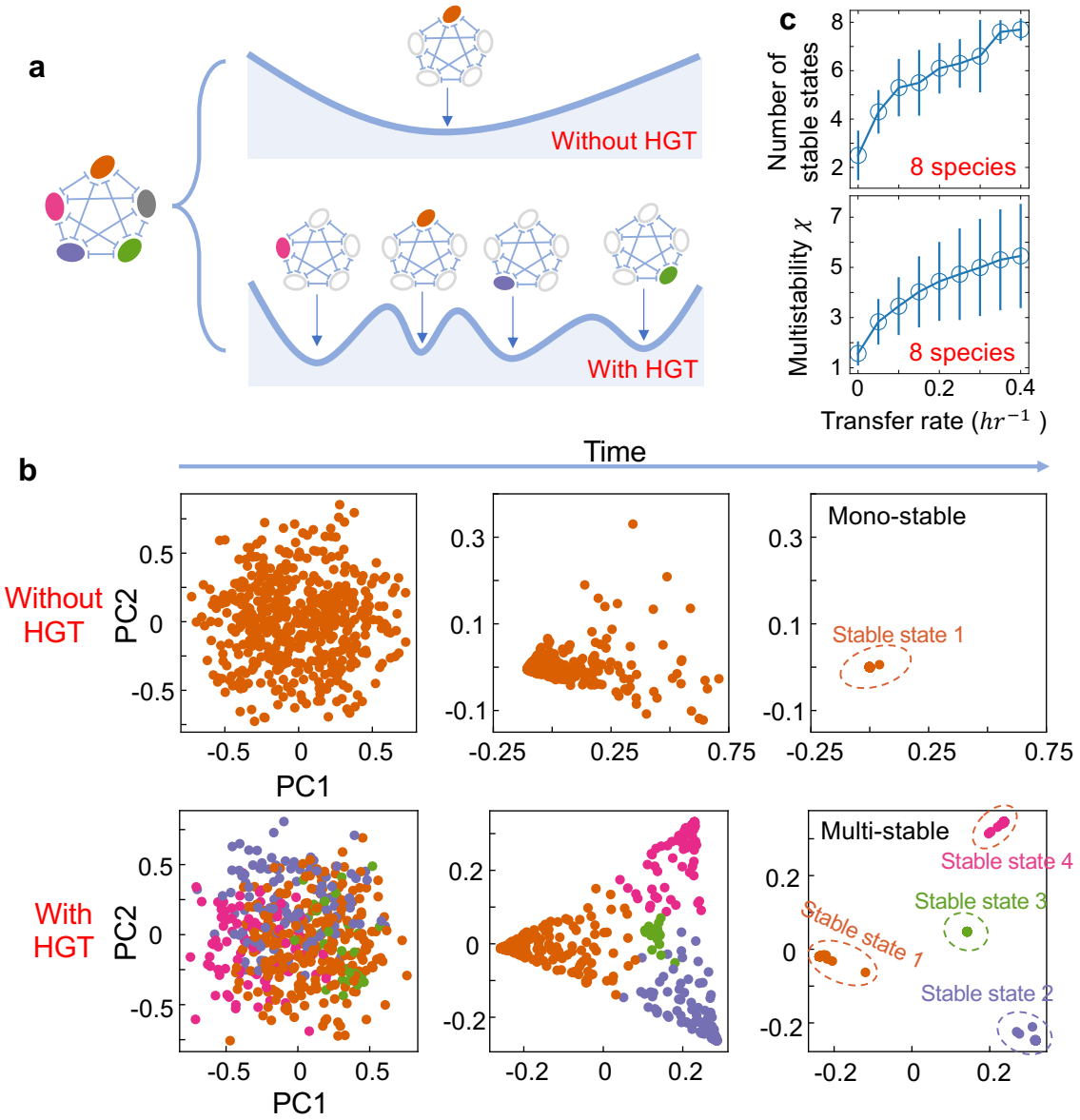

Fig. 2| The number of alternative stable states in multi-species communities increases with HGT rate.

(a), A schematic of the stability landscape of a population composed of multiple competing species with or without HGT. Each alternative stable state is characterized by a different dominant species (shown in filled circles).

(b), The emergence of alternative stable states in a five-species community with gene transfer. We simulated the dynamics of 500 parallel communities, each with the same kinetic parameters but

different initial compositions. The species compositions of these communities at three different timepoints were shown by principal component analysis from left to right. Without HGT ($\eta = 0$), all populations converged into a single stable state. In contrast, with HGT ($\eta = 0.2\ hr^{-1}$), four different dynamic attractors coexist. Here, populations reaching different stable states were marked with different colors. Other parameters are $\mu_1^0 = \mu_2^0 = \mu_3^0 = \mu_4^0 = \mu_5^0 = 0.5\ hr^{-1}$, $\mu_1 = 0.52\ hr^{-1}$, $\mu_2 = 0.48\ hr^{-1}$, $\mu_3 = 0.44\ hr^{-1}$, $\mu_4 = 0.60\ hr^{-1}$, $\mu_5 = 0.31\ hr^{-1}$, $\gamma = 1.05$, $\kappa = 0.005\ hr^{-1}$, $D = 0.2\ hr^{-1}$.

(c), The number of stable states (top panel) and the multistability coefficient χ increase with HGT rate in communities consisting of 8 competing species. We calculated the number of stable states by randomly initializing the species abundances 500 times between 0 and 1 following uniform distributions. Then we simulated the steady states and clustered them into different attractors by applying a threshold of 0.05 on their Euclidean distances. The data were presented as mean $\pm$ standard deviation of 10 replicates. Each replicate corresponded to a different combination of randomized species growth rates.

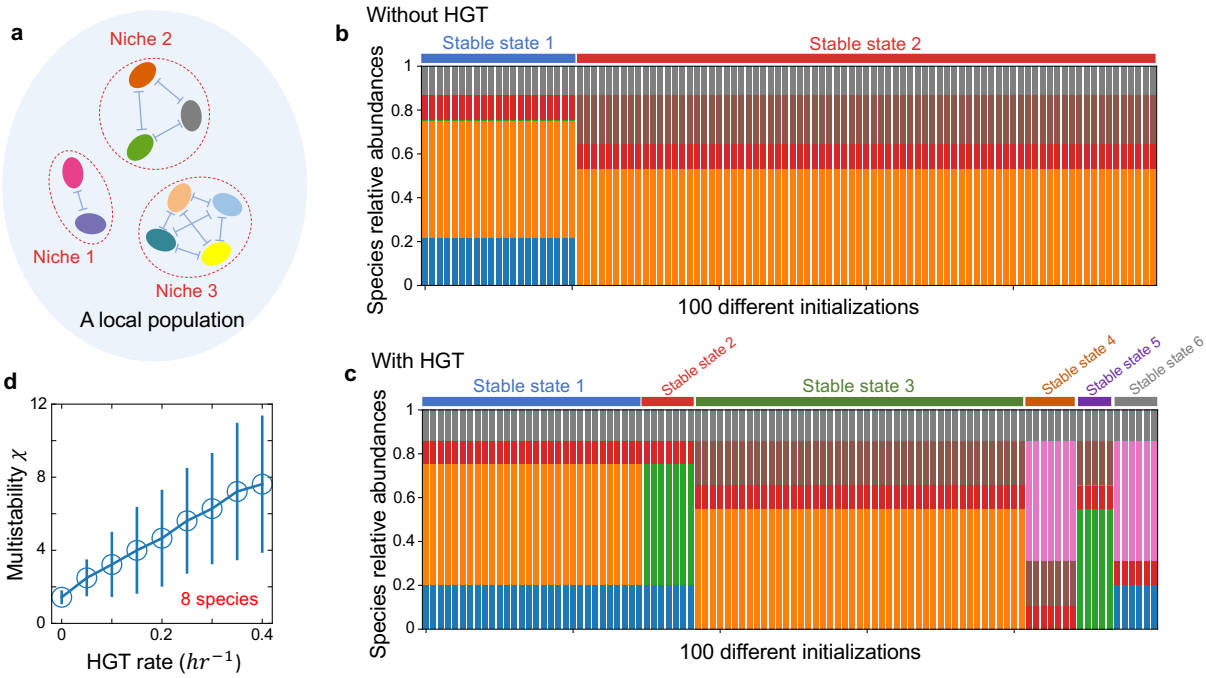

Fig. 3| HGT promotes the multistability of communities with multiple niches.

(a), A schematic of a microbial population consisting of multiple niches. Species within each niche share the same carrying capacity and compete with each other, while species from different niches can coexist.

(**b-c),** Multiple alternative stable states emerge in niche communities with gene exchange. Here, a system consisting of 10 species and 4 niches were shown as examples. The steady-state compositions of 100 parallel populations, each with different initializations, were calculated with ($\eta = 0.1\ hr^{-1}$) or without HGT. The heights of the colored bars represent the relative abundances of different species. Without HGT, 2 stable states existed for the 100 populations, while with HGT, 6 different stable states existed. The carrying capacity of each niche was randomized between 0 and 1. Other parameters are $\mu_i^0 = 0.5\ hr^{-1}$, $\kappa = 0.005\ hr^{-1}$, $D = 0.2\ hr^{-1}$. Interspecies competition strength equals 1.05 within each niche.

(d), The multistability χ in niche communities increases with HGT rate. Communities of 8 species were considered as an example. The data were presented as mean $\pm$ standard deviation

of 10 replicates. For each replicate, the species growth rates were randomized between 0.3 and 0.7 hr^{-1} following uniform distributions. The number of niches were randomized as 2, 3 or 4.

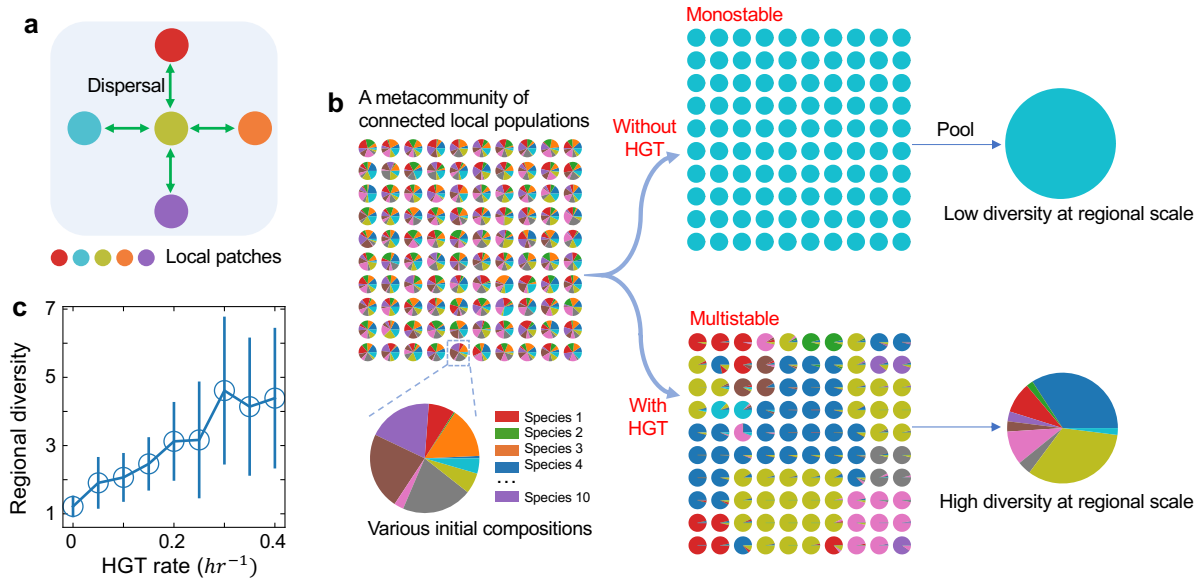

Fig. 4| HGT promotes the regional diversity in metacommunities of local populations connected by dispersal.

(a), A schematic of microbial dispersal within the metacommunity. The filled circles represent different local patches.

(b), A metacommunity composed of 100 connected patches was shown as an example. Each local population contained 10 competing species and was randomly initialized with different species compositions. Dispersal occurred between neighboring patches with a rate of 0.001 hr^{-1}. Without HGT, the systems were monostable, resulting in low regional diversity. HGT promotes the regional diversity by the emergence of multistability in each local patch. The collective diversity of the metacommunity was calculated by pooling all the local populations together. Other parameters are $\mu_i^0 = 0.5\ hr^{-1},\ \gamma = 1.05,\ \kappa = 0.005\ hr^{-1},\ D = 0.2\ hr^{-1}$.

(c), The regional diversity of a metacommunity increases with HGT rate. We first pooled all local populations together and calculated the total abundance of every species in the metacommunity. Then we quantified the regional diversity using Shannon index. The data were presented as mean $\pm$ standard deviation of 10 replicates.

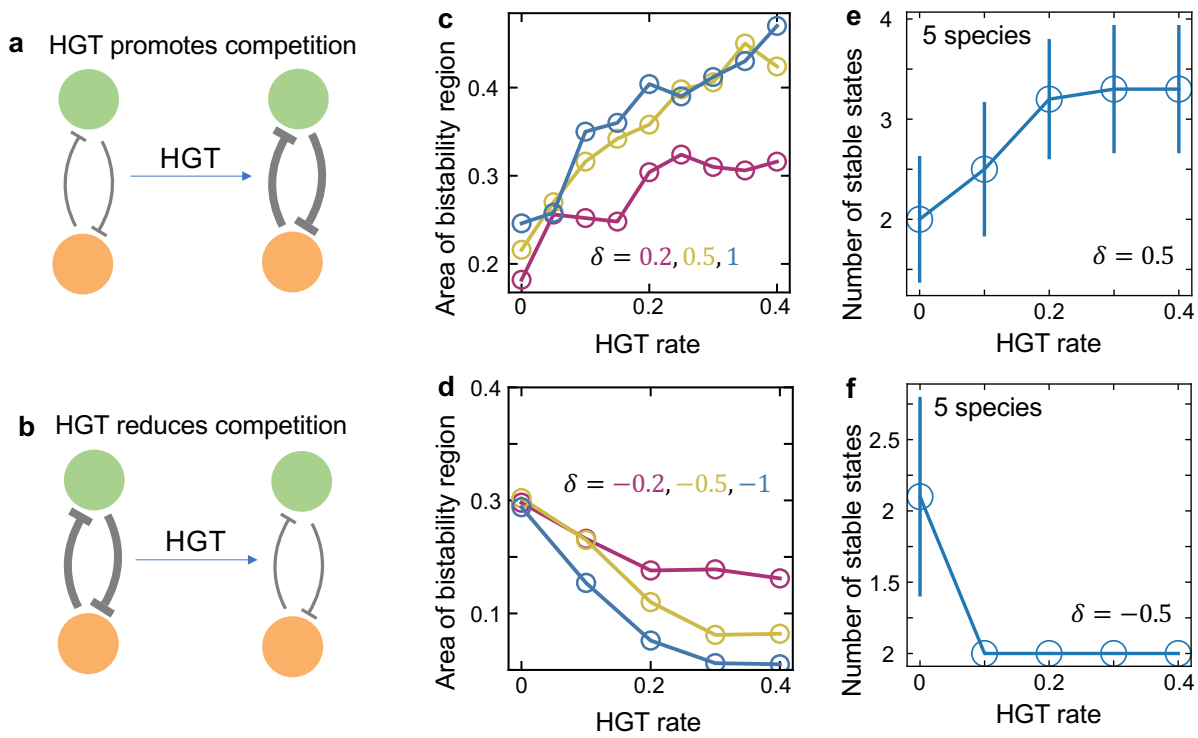

Fig.5| The effects of HGT on population multistability when MGEs promote or reduce competition.

(a-b), The schematics of HGT promoting or reducing competition.

(c), For populations of two species, when MGEs promote competition, increasing HGT rate enlarged the area of bistability region in the phase diagram. Here, δ describes the effect of mobile genes on the competition strength. Positive δ represents HGT promoting competition. In numerical simulations, we tested three different δ values (marked in different colors). When calculating the area of bistability region, we randomized μ_1 and μ_2 500 times between 0 and 1 hr^{-1} following uniform distributions while keeping μ_1^0 and μ_2^0 constants. For each pair of growth rates, we randomized the initial abundance of each species 200 times between 0 and 1 following uniform distributions. The system was monostable if all initializations led to the same steady state. Otherwise, the system was bistable. Then we calculated the fraction of growth rate combinations that generated bistability out of the 500 random combinations. Other parameters are $\gamma_1 = \gamma_2 = 1.1$, $\kappa = 0.005\ h^{-1}$, $D = 0.2\ h^{-1}$.

(d), When MGEs reduce competition, the area of bistability region decreases with HGT rate. Three negative δ values were tested and shown as examples here.

(e), For populations of 5 species, when MGEs promote competition, the number of stable states increases with HGT rate. We calculated the number of stable states by randomly initializing the species abundances 500 times. Then we simulated the steady states and clustered them into different attractors by applying a threshold of 0.05 on their Euclidean distances. The data were presented as mean $\pm$ standard deviation of 10 replicates. Each replicate corresponds to a different combination of randomized species growth rates. Other parameters are $\gamma_{i,j} = 1.1$, $\kappa = 0.005\ h^{-1}$, $D = 0.2\ h^{-1}, \delta = 0.5$.

(f), When MGEs reduce competition, the number of stable states decrease with HGT rate. The data were presented as mean $\pm$ standard deviation of 10 replicates. $\delta = -0.5$ was used in the simulation.

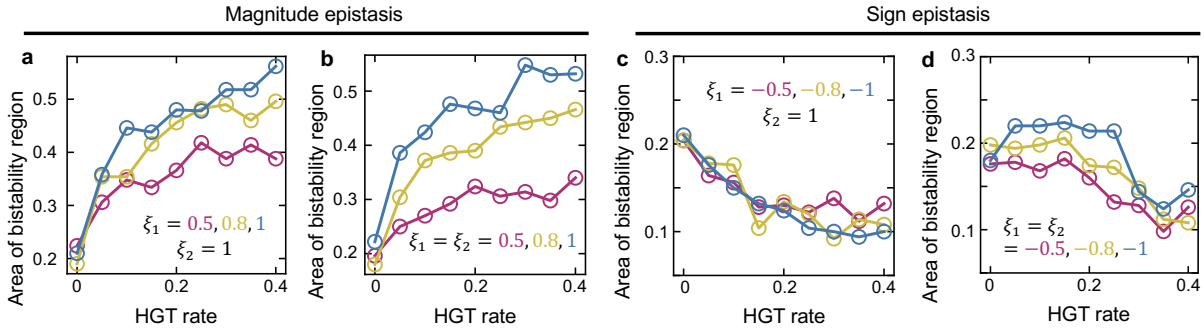

Fig. 6| The influence of epistasis on the role of HGT in mediating population bistability.

(a-b) With magnitude epistasis, increasing HGT rate still promotes bistability in populations of two competing species.

(c-d) With sign epistasis, increasing HGT rate reduces the area of bistability region. For each type of epistasis, we considered two scenarios. In a and c, host genetic background influences the fitness effect of only one MGE, while in b and d, host genetic background influences both MGEs. ξ_1 and ξ_2 are defined as $\lambda_{21}/\lambda_{11}$ and $\lambda_{12}/\lambda_{22}$, respectively. $\xi_1 > 0$ and $\xi_2 > 0$ represent magnitude epistasis, while $\xi_1 < 0$ or $\xi_2 < 0$ represents the sign epistasis. Other parameters are $\gamma_1 = \gamma_2 = 1.1$, $\kappa = 0.005\ h^{-1}$, $D = 0.2\ h^{-1}$.

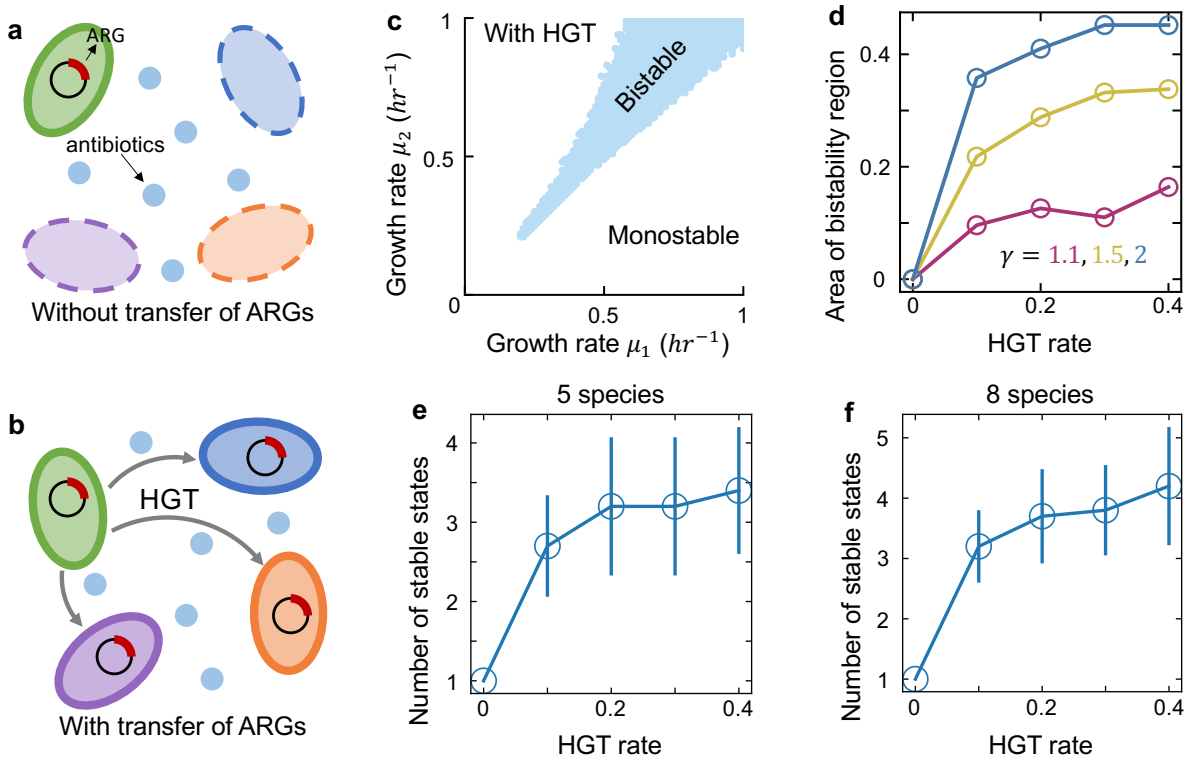

Fig. 7| The horizontal transfer of ARGs creates chances of multistability for communities under strong antibiotic selection.

(a-b), The schematics of communities under strong antibiotic selection. Without HGT, only the donor species carrying the ARG can survive. HGT allows the other species to acquire ARG from the donor, creating opportunities for the other species to survive under antibiotic treatments.

(c), The phase diagram of two-species populations transferring an ARG. Different combinations of μ_1 and μ_2 between 0 and 1 hr^{-1} were tested. All combinations of μ_1 and μ_2 that led to bistability were marked in blue in the diagram. Other parameters are $\gamma = 1.1$, $\kappa = 0.005\ hr^{-1}$, $D = 0.2\ hr^{-1}$, $\mu_1^0 = \mu_2^0 = 0.5\ hr^{-1}$. Here, we assumed that the ARG was initially carried only by species 1. Bistability was more feasible when $\mu_2 > \mu_1$.

(d), Increasing HGT rate enlarges the area of bistability region in the phase diagram of two competing species transferring an ARG. Three different competition strengths were tested (marked in different colors).

(e-f), For communities of 5 or 8 species under antibiotic selection, increasing HGT rate of an ARG promotes the emergence of alternative stable states. We calculated the number of stable states by

randomly initializing the species abundances 500 times. Then we simulated the steady states and clustered them into different attractors. The data were presented as mean $\pm$ standard deviation of 10 replicates. Each replicate corresponds to a different combination of randomized species growth rates. Other parameters are $\gamma_{i,j} = 1.5,\ \kappa = 0.005\ h^{-1},\ D = 0.2\ h^{-1}$.

Methods

Modeling framework of two competing species sharing mobile genes

We used a mathematical model developed in a previous work to analyze the population dynamics of two competing species transferring mobile genes with fitness effects[27]. Briefly, the model includes four ordinary differential equations (ODEs):

$$\frac{dS_1}{dt} = \mu_1^e S_1 \left(1 - \frac{S_1 + \gamma_2 S_2}{N_m}\right) - DS_1, \quad (1)$$

$$\frac{dS_2}{dt} = \mu_2^e S_2 \left(1 - \frac{S_2 + \gamma_1 S_1}{N_m}\right) - DS_2, \quad (2)$$

$$\frac{dP_1}{dt} = \mu_1(1+\lambda_2)P_1 \left(1 - \frac{S_1 + \gamma_2 S_2}{N_m}\right) + \eta_1^c(S_2 + P_1)(S_1 - P_1) - (D + \kappa_1)P_1, \quad (3)$$

$$\frac{dP_2}{dt} = \mu_2(1+\lambda_1)P_2 \left(1 - \frac{S_2 + \gamma_1 S_1}{N_m}\right) + \eta_2^c(S_1 + P_2)(S_2 - P_2) - (D + \kappa_2)P_2. \quad (4)$$

S_1 and S_2 are the abundances of the two species. γ_1 and γ_2 describe the strengths of interspecies competition. N_m is the maximum carrying capacity, and D is the dilution rate. P_i $(i = 1, 2)$ represents the abundance of the subpopulation in the i-th species that acquires the mobilizable genes from its competitor. μ_i represents the maximum growth rate of the i-th species when interspecies HGT is absent. μ_i is calculated as $\mu_i = \mu_i^0(1 + \lambda_i)$ where μ_i^0 is the basal growth rate determined by the non-mobilizable genes and λ_i is the fitness effect of the mobile genes. Interspecies gene flow allows each species to acquire mobile genes from its competitor, resulting in the dynamic change of the effective species growth rates μ_i^e, which is calculated as: $\mu_1^e = \mu_1(1 + \lambda_2 \frac{P_1}{S_1})$ and $\mu_2^e = \mu_2(1 + \lambda_1 \frac{P_2}{S_2})$. η_1^c and η_2^c stand for HGT rates. Here, we assumed that intraspecies and interspecies transfer occurred at the same rates. κ_1 and κ_2 are the loss rates of the mobile genes.

Let $s_1 = S_1/N_m$, $s_2 = S_2/N_m$, $p_1 = P_1/N_m$ and $p_2 = P_2/N_m$. The model can be further simplified as

$$\frac{ds_1}{dt} = \mu_1^e s_1(1 - s_1 - \gamma_2 s_2) - Ds_1, \quad (5)$$

$$\frac{ds_2}{dt} = \mu_2^e s_2(1 - s_2 - \gamma_1 s_1) - Ds_2, \quad (6)$$

$$\frac{dp_1}{dt} = \mu_1(1 + \lambda_2)p_1(1 - s_1 - \gamma_2 s_2) + \eta_1(s_2 + p_1)(s_1 - p_1) - (D + \kappa_1)p_1, \quad (7)$$

$$\frac{dp_2}{dt} = \mu_2(1 + \lambda_1)p_2(1 - s_2 - \gamma_1 s_1) + \eta_2(s_1 + p_2)(s_2 - p_2) - (D + \kappa_2)p_2. \quad (8)$$

Here, s_1, s_2, p_1 and p_2 are dimensionless. η_i is related with η_i^c by $\eta_i = N_m \eta_i^c$. Therefore, the unit of η_1 and η_2 is $hour^{-1}$. Without HGT, p_1 and p_2 become consistently 0, and the model is equivalent to the classic Lotka-Volterra (LV) framework:

$$\frac{ds_1}{dt} = \mu_1 s_1(1 - s_1 - \gamma_2 s_2) - Ds_1, \quad (9)$$

$$\frac{ds_2}{dt} = \mu_2 s_2(1 - s_2 - \gamma_1 s_1) - Ds_2. \quad (10)$$

Stability analysis of the classic LV model

The classic LV model has four fixed points: $\mathcal{g}_1 = [0, 0]$, $\mathcal{g}_2 = [0, 1 - \frac{D}{\mu_2}]$, $\mathcal{g}_3 = [1 - \frac{D}{\mu_1}, 0]$, $\mathcal{g}_4 = [\frac{\gamma_2\mu_1\mu_2 - D\gamma_2\mu_1 - \mu_1\mu_2 + D\mu_2}{\mu_1\mu_2(\gamma_1\gamma_2 - 1)}, \frac{\gamma_1\mu_1\mu_2 - D\gamma_1\mu_2 - \mu_1\mu_2 + D\mu_1}{\mu_1\mu_2(\gamma_1\gamma_2 - 1)}]$. The Jacobian matrix of each fixed point can be calculated as $J = \begin{bmatrix} \mu_1 - 2\mu_1 s_1^* - \mu_1\gamma_2 s_2^* - D & -\mu_1\gamma_2 s_1^* \\ -\mu_2\gamma_1 s_2^* & \mu_2 - 2\mu_2 s_2^* - \mu_2\gamma_1 s_1^* - D \end{bmatrix}$, where s_1^* and s_2^* are the species abundances at each fixed point.

The system is bistable only when $\mathcal{g}_2$ and $\mathcal{g}_3$ are both stable. The Jacobian matrix of $\mathcal{g}_2$ is $J_2 = \begin{bmatrix} \mu_1 - D - \mu_1\gamma_2 + \frac{\mu_1\gamma_2 D}{\mu_2} & 0 \\ -\mu_2\gamma_1 + D\gamma_1 & D - \mu_2 \end{bmatrix}$. The eigenvalues of J_2 can be obtained as $\mu_1 - D - \mu_1\gamma_2 + \frac{\mu_1\gamma_2 D}{\mu_2}$ and $D - \mu_2$. $\mathcal{g}_2$ is stable when both eigenvalues are negative, which leads to $\gamma_2 > \phi_1/\phi_2$ where $\phi_1 = \frac{\mu_1 - D}{\mu_1}$ and $\phi_2 = \frac{\mu_2 - D}{\mu_2}$. Similarly, $\mathcal{g}_3$ is stable when $\gamma_1 > \phi_2/\phi_1$. Therefore, the condition for the system being bistable is $\gamma_2 > \phi_1/\phi_2$ and $\gamma_1 > \phi_2/\phi_1$.

Bistability analysis of two-species populations by numerical simulations

We performed numerical simulations to determine the bistability of a population consisting of two competing species transferring mobile genes. Specifically, for a system with given parameters, we randomly initialized the species abundances between 0 and 1 following uniform distributions for 200 times. Then we simulated the dynamics of each population till the abundance of every species reached equilibrium, and we treated it as a steady state. We grouped the 200 steady states into different attractors by applying the threshold of 0.01. Two steady states with their Euclidean distance smaller than the threshold belonged to the same group. The Euclidean distance was calculated as $d_{ij} = \sqrt{\sum_{k=1}^{m}(s_{i,k} - s_{j,k})^2}$ where k is the species index and $s_{i,k}$ represents the abundance of the k-th species in the i-th steady state.

Theoretical framework of multiple competing species transferring mobile genes

For a community of m competing species that share mobile genes with each other, the modeling framework consists of two groups of ODEs:

$$\frac{ds_i}{dt} = \mu_i^e s_i \left(1 - s_i - \sum_{j \neq i} \gamma_{ji}\, s_j\right) - D s_i, \quad (11)$$

$$\frac{dp_{ij}}{dt} = \mu_i(1 + \lambda_{ij}) \left[\prod_{k \neq i,j} \left(1 + \lambda_{ik} \frac{p_{ik}}{s_i}\right)\right] p_{ij} \left(1 - s_i - \sum_{j \neq i} \gamma_{ji}\, s_j\right) + (s_i - p_{ij}) \sum_{k=1}^{n} \eta_{jki} p_{kj} - (D + \kappa_{ij}) p_{ij}. \ (i \neq j). \quad (12)$$

s_i is the abundance of the i-th species. p_{ij} is the size of the subpopulation in the i-th species that acquires s_j-originated mobile genes. γ_{ji} is the negative interaction that s_j imposes on the i-th species. D is the dilution rate. μ_i^e, the effective growth rate of s_i, is calculated by $\mu_i^e = \mu_i \prod_{j \neq i} \left(1 + \lambda_{ij} \frac{p_{ij}}{s_i}\right)$. μ_i is defined as $\mu_i = \mu_i^0 (1 + \lambda_{ii})$ where μ_i^0 is the basal growth rate, λ_{ij} is the fitness effect of the s_j-originated mobile genes in the i-th species. η_{jki} is the transfer rate of the s_j-originated genes from species k to species i. κ_{ij} is the gene loss rate.

Analysis of multistability of complex communities

For a population of m species with given niches and kinetic parameters, we initialized the system 500 times in the ranges of $0 < s_i < 1$ following uniform distributions. The initial conditions for p_{ij}'s are $p_{ii} = s_i$ and $p_{ij} = 0$ $(i \neq j)$. Then the dynamics of each population was simulated for 2000 hours till the system reached the steady state. For each steady state we obtained the corresponding species composition and grouped the 500 solutions into different stable states based on their Euclidean distances.

Niche-based model of multi-species communities

For a community consisting of m competing species, let the number of niches be l. Each niche has a maximum carrying capacity $N_m^{(i)}$ $(i = 1,2,\dots,l)$. Each species lives in one of the niches. Let M be the map from species index to the index of its niche. $M_i = k$ means that the i-th species lives in the k-th niche. For species i and j, if $M_i = M_j$, these two species belong to the same niche and compete with each other. Species from different niche do not directly interact. Therefore, the model becomes:

$$\frac{dS_i}{dt} = \mu_i^e S_i \left(1 - \frac{S_i + \sum_{\{j:\, M_j = M_i\}} \gamma_{ji}\, s_j}{N_m^{(M_i)}}\right) - DS_i, \quad (13)$$

$$\frac{dP_{ij}}{dt} = \mu_i(1+\lambda_{ij})\left[\prod_{k\neq i,j}\left(1+\lambda_{ik}\frac{P_{ik}}{s_i}\right)\right]P_{ij}\left(1 - \frac{S_i + \sum_{\{j:\, M_j = M_i\}} \gamma_{ji}\, s_j}{N_m^{(M_i)}}\right) + (S_i - P_{ij})\sum_{k=1}^{n}\eta_{jki}P_{kj} - (D+\kappa_{ij})P_{ij}. \quad (i \neq j). \quad (14)$$

In simulations, the number of niches was randomized between 2 and $m/2$. The maximum carrying capacity of each niche was randomized between 0 and 1 following uniform distributions. Then each species was randomly allocated into one of the niches.

Theoretical framework of metacommunity dynamics

Consider a metacommunity composed of $u \times v$ local patches. The location of each patch can be described by two coordinates $[a, b]$ ($a = 1,2,\dots,u$ and $b = 1,2,\dots,v$). Let ω be the

dispersal rate between the adjacent patches. The dynamics of the metacommunity can then be described by generalizing equations (11) and (12) to each local patch:

$$\frac{ds_{a,b,i}}{dt} = \mu^{e}_{a,b,i} s_{a,b,i}\left(1 - s_{a,b,i} - \sum_{j\neq i}\gamma_{ji}\, s_{a,b,j}\right) - D s_{a,b,i} + \mathcal{H}_{s}^{(a,b)}, \quad (15)$$

$$\frac{dp_{a,b,i,j}}{dt} = \mu_i\left(1+\lambda_{ij}\right)\left[\prod_{k\neq i,j}\left(1+\lambda_{ik}\frac{p_{a,b,i,k}}{s_{a,b,i}}\right)\right] p_{a,b,i,j}\left(1 - s_{a,b,i} - \sum_{j\neq i}\gamma_{ji}\, s_{a,b,j}\right)$$

$$+\left(s_{a,b,i} - p_{a,b,i,j}\right)\sum_{k=1}^{n}\eta_{jki} p_{a,b,k,j} - \left(D+\kappa_{ij}\right)p_{a,b,i,j} + \mathcal{H}_{p}^{(a,b)}. \ (i \neq j). \quad (16)$$

For the patch located at $[a, b]$, $s_{a,b,i}$ is the abundance of the i-th species, and $p_{a,b,i,j}$ is the size of the subpopulation in the i-th species that acquires s_j-originated mobile genes. The effective growth rate $\mu^{e}_{a,b,i}$ is calculated as $\mu^{e}_{a,b,i} = \mu_i \prod_{j\neq i}\left(1+\lambda_{ij}\frac{p_{a,b,i,j}}{s_{a,b,i}}\right)$.

$\mathcal{H}_{s}^{(a,b)}$ and $\mathcal{H}_{p}^{(a,b)}$ are the gains of $s_{a,b,i}$ and $p_{a,b,i,j}$ by dispersal, respectively. We assumed that microbial dispersal only occurred between adjacent patches. Therefore, $\mathcal{H}_{s}^{(a,b)}$ was calculated by summing the dispersal terms at four directions: left, right, up, and down. The left component can be calculated as

$$\mathcal{H}_{s,left}^{(a,b)} = \begin{cases} \omega\left(s_{a-1,b,i} - s_{a,b,i}\right), if\ a-1>0 \\ 0, if\ a-1 \leq 0 \end{cases}.$$

Similarly, $\mathcal{H}_{s,right}^{(a,b)}$, $\mathcal{H}_{s,up}^{(a,b)}$ and $\mathcal{H}_{s,down}^{(a,b)}$ is calculated as:

$$\mathcal{H}_{s,right}^{(a,b)} = \begin{cases} \omega\left(s_{a+1,b,i} - s_{a,b,i}\right), if\ a+1<u+1 \\ 0, if\ a+1 \geq u+1 \end{cases},$$

$$\mathcal{H}_{s,up}^{(a,b)} = \begin{cases} \omega\left(s_{a,b+1,i} - s_{a,b,i}\right), if\ b+1<v+1 \\ 0, if\ b+1 \geq v+1 \end{cases}$$

$$\mathcal{H}_{s,down}^{(a,b)} = \begin{cases} \omega\left(s_{a,b-1,i} - s_{a,b,i}\right), if\ b-1>0 \\ 0, if\ b-1 \leq 0 \end{cases}.$$

$\mathcal{H}_s^{(a,b)}$ can then be obtained as $\mathcal{H}_{s,left}^{(a,b)} + \mathcal{H}_{s,right}^{(a,b)} + \mathcal{H}_{s,up}^{(a,b)} + \mathcal{H}_{s,down}^{(a,b)}$. $\mathcal{H}_p^{(a,b)}$ can be formulated in the similar way.

The collective species diversity in a metacommunity

To analyze the total species diversity in a metacommunity, we first calculated the total abundance of each species across all patches: $s_i = \sum_{a=1,2,\ldots,u} \sum_{b=1,2,\ldots,v} s_{a,b,i}$. Then we measured the diversity using Shannon index, a common metric used in ecology. Shannon index can be calculated as $exp\ [-\sum_{i=1}^{m} \frac{s_i}{s_T} log \frac{s_i}{s_T}]$. s_T is the total species abundance: $s_T = \sum_{i=1}^{m} s_i$.

Biological relevance of our analysis

The empirically measured gene transfer rates (denoted as η^c, with the unit of $cells^{-1} \cdot mL \cdot hour^{-1}$) should be multiplied by N_m, the maximum carrying capacity of the population, before being used our model. Therefore, the transfer rate η in our analysis are several orders of magnitude higher than the experimentally measured rates[51,52]. In this work, we focused on HGT rate in the range of $0 < \eta_i < 0.4\ hour^{-1}$. Whether this range is biologically relevant depends on N_m of the population. Considering the typical estimates of plasmid transfer rates cross species ($10^{-13}\ cells^{-1} \cdot mL \cdot hour^{-1}$, from *Klebsiella pneumoniae* to *Escherichia coli*) and within species ($10^{-7}\ cells^{-1} \cdot mL \cdot hour^{-1}$, between *E. coli* strains) provided by a previous study[51], HGT rates in our analysis are relevant in various environments from human colon (~10^{12} cells per gram) [53] to deep oceanic subsurface (10^6~10^8 cells per gram)[54].

References

1 Gonze, D., Lahti, L., Raes, J. & Faust, K. Multi-stability and the origin of microbial community types. *The ISME Journal* **11**, 2159-2166 (2017).

2 Arumugam, M. *et al.* Enterotypes of the human gut microbiome. *Nature* **473**, 174-180 (2011).

3 Gibson, T. E., Bashan, A., Cao, H.-T., Weiss, S. T. & Liu, Y.-Y. On the origins and control of community types in the human microbiome. *PLoS Computational Biology* **12**, e1004688 (2016).

4 Estrela, S. *et al.* Functional attractors in microbial community assembly. *Cell Systems* **13**, 29-42. e27 (2022).

5 Chaparro-Pedraza, P. C. & de Roos, A. M. Ecological changes with minor effect initiate evolution to delayed regime shifts. *Nature Ecology and Evolution* **4**, 412-418 (2020).

6 Beardmore, R. E. *et al.* Drug-mediated metabolic tipping between antibiotic resistant states in a mixed-species community. *Nature Ecology and Evolution* **2**, 1312-1320 (2018).

7 Amor, D. R., Ratzke, C. & Gore, J. Transient invaders can induce shifts between alternative stable states of microbial communities. *Science Advances* **6**, eaay8676 (2020).

8 Relman, D. A. The human microbiome: ecosystem resilience and health. *Nutrition Reviews* **70**, S2-S9 (2012).

9 Hartmann, M. & Six, J. Soil structure and microbiome functions in agroecosystems. *Nature Reviews Earth and Environment* **4**, 4-18 (2023).

10 Sun, L. *et al.* The shift of soil microbial community induced by cropping sequence affect soil properties and crop yield. *Frontiers in Microbiology* **14**, 1095688 (2023).

11 Kumar, S. & Hasty, J. Stability, robustness, and containment: preparing synthetic biology for real-world deployment. *Current Opinion in Biotechnology* **79**, 102880 (2023).

12 Fuhrman, J. A., Cram, J. A. & Needham, D. M. Marine microbial community dynamics and their ecological interpretation. *Nature Reviews Microbiology* **13**, 133-146 (2015).

13 Khazaei, T. *et al.* Metabolic multistability and hysteresis in a model aerobe-anaerobe microbiome community. *Science Advances* **6**, eaba0353 (2020).

14 Dubinkina, V., Fridman, Y., Pandey, P. P. & Maslov, S. Multistability and regime shifts in microbial communities explained by competition for essential nutrients. *Elife* **8**, e49720 (2019).

15 Fujita, H. *et al.* Alternative stable states, nonlinear behavior, and predictability of microbiome dynamics. *Microbiome* **11**, 63 (2023).

16 Mangal, U. *et al.* Multistability and hysteresis in states of oral microbiota: Is it impacting the dental clinical cohort studies? *Journal of Periodontal Research* **58**, 381-391 (2023).

17 Zaoli, S. & Grilli, J. A macroecological description of alternative stable states reproduces intra-and inter-host variability of gut microbiome. *Science Advances* **7**, eabj2882 (2021).

18 Fassarella, M. *et al.* Gut microbiome stability and resilience: elucidating the response to perturbations in order to modulate gut health. *Gut* **70**, 595-605 (2021).

19 Andersson, D. I. & Hughes, D. Antibiotic resistance and its cost: is it possible to reverse resistance? *Nature Reviews Microbiology* **8**, 260-271 (2010).

20 van den Berg, N. I. *et al.* Ecological modelling approaches for predicting emergent properties in microbial communities. *Nature Ecology and Evolution* **6**, 855-865 (2022).

21 Soucy, S. M., Huang, J. & Gogarten, J. P. Horizontal gene transfer: building the web of life. *Nature Reviews Genetics* **16**, 472-482 (2015).
22 Bordenstein, S. R. & Reznikoff, W. S. Mobile DNA in obligate intracellular bacteria. *Nature Reviews Microbiology* **3**, 688-699 (2005).
23 Brito, I. L. *et al.* Mobile genes in the human microbiome are structured from global to individual scales. *Nature* **535**, 435-439 (2016).
24 Brockhurst, M. A. *et al.* The ecology and evolution of pangenomes. *Current Biology* **29**, R1094-R1103 (2019).
25 Smillie, C. S. *et al.* Ecology drives a global network of gene exchange connecting the human microbiome. *Nature* **480**, 241-244 (2011).
26 Gilpin, M. E. & CASE, T. J. Multiple domains of attraction in competition communities. *Nature* **261**, 40-42 (1976).
27 Zhu, S., Hong, J. & Wang, T. Horizontal gene transfer is predicted to overcome the diversity limit of competing microbial species. *Nature Communications* **15**, 800, doi:10.1038/s41467-024-45154-w (2024).
28 Finlay, B. B. & Medzhitov, R. Host-microbe interactions: fulfilling a niche. *Cell Host and Microbe* **1**, 3-4 (2007).
29 Leibold, M. A. *et al.* The metacommunity concept: a framework for multi-scale community ecology. *Ecology Letters* **7**, 601-613 (2004).
30 Miller, E. T., Svanbäck, R. & Bohannan, B. J. Microbiomes as metacommunities: understanding host-associated microbes through metacommunity ecology. *Trends in Ecology and Evolution* **33**, 926-935 (2018).
31 Bonham, K. S., Wolfe, B. E. & Dutton, R. J. Extensive horizontal gene transfer in cheese-associated bacteria. *Elife* **6**, e22144 (2017).
32 Caro-Quintero, A. & Konstantinidis, K. T. Inter-phylum HGT has shaped the metabolism of many mesophilic and anaerobic bacteria. *The ISME journal* **9**, 958-967 (2015).
33 Mc Ginty, S. É., Lehmann, L., Brown, S. P. & Rankin, D. J. The interplay between relatedness and horizontal gene transfer drives the evolution of plasmid-carried public goods. *Proceedings of the Royal Society B: Biological Sciences* **280**, 20130400 (2013).
34 Dimitriu, T. *et al.* Genetic information transfer promotes cooperation in bacteria. *Proceedings of the National Academy of Sciences* **111**, 11103-11108 (2014).
35 Acar Kirit, H., Lagator, M. & Bollback, J. P. Experimental determination of evolutionary barriers to horizontal gene transfer. *BMC Microbiology* **20**, 1-13 (2020).
36 Gama, J. A., Zilhão, R. & Dionisio, F. Plasmid interactions can improve plasmid persistence in bacterial populations. *Frontiers in Microbiology* **11**, 2033 (2020).
37 Silva, R. F. *et al.* Pervasive sign epistasis between conjugative plasmids and drug-resistance chromosomal mutations. *PLoS Genetics* **7**, e1002181 (2011).
38 San Millan, A., Heilbron, K. & MacLean, R. C. Positive epistasis between co-infecting plasmids promotes plasmid survival in bacterial populations. *The ISME Journal* **8**, 601-612 (2014).
39 Serván, C. A., Capitán, J. A., Grilli, J., Morrison, K. E. & Allesina, S. Coexistence of many species in random ecosystems. *Nature Ecology and Evolution* **2**, 1237-1242 (2018).

40 Grilli, J. *et al.* Feasibility and coexistence of large ecological communities. *Nature Communications* **8**, 14389 (2017).
41 Liu, L. *et al.* The human microbiome: a hot spot of microbial horizontal gene transfer. *Genomics* **100**, 265-270 (2012).
42 Kosterlitz, O. *et al.* Estimating the transfer rates of bacterial plasmids with an adapted Luria–Delbrück fluctuation analysis. *PLoS Biology* **20**, e3001732 (2022).
43 Ravel, J. *et al.* Vaginal microbiome of reproductive-age women. *Proceedings of the National Academy of Sciences* **108**, 4680-4687 (2011).
44 Ding, T. & Schloss, P. D. Dynamics and associations of microbial community types across the human body. *Nature* **509**, 357-360 (2014).
45 Lahti, L., Salojärvi, J., Salonen, A., Scheffer, M. & De Vos, W. M. Tipping elements in the human intestinal ecosystem. *Nature Communications* **5**, 4344 (2014).
46 Kootte, R. S. *et al.* Improvement of insulin sensitivity after lean donor feces in metabolic syndrome is driven by baseline intestinal microbiota composition. *Cell Metabolism* **26**, 611-619. e616 (2017).
47 Canfora, E. E., Meex, R. C., Venema, K. & Blaak, E. E. Gut microbial metabolites in obesity, NAFLD and T2DM. *Nature Reviews Endocrinology* **15**, 261-273 (2019).
48 Moustafa, A. *et al.* Genetic risk, dysbiosis, and treatment stratification using host genome and gut microbiome in inflammatory bowel disease. *Clinical Translational Gastroenterology* **9**, e132 (2018).
49 Palencia-Gándara, C. *et al.* Conjugation inhibitors effectively prevent plasmid transmission in natural environments. *MBio* **12**, 10.1128/mbio. 01277-01221 (2021).
50 Fernandez-Lopez, R. *et al.* Unsaturated fatty acids are inhibitors of bacterial conjugation. *Microbiology* **151**, 3517-3526 (2005).
51 Kosterlitz, O. *et al.* Estimating the transfer rates of bacterial plasmids with an adapted Luria–Delbrück fluctuation analysis. *PLoS Biology* **20**, e3001732 (2022).
52 Lopatkin, A. J. *et al.* Persistence and reversal of plasmid-mediated antibiotic resistance. *Nature Communications* **8**, 1689 (2017).
53 Dieterich, W., Schink, M. & Zopf, Y. Microbiota in the gastrointestinal tract. *Medical Sciences* **6**, 116 (2018).
54 Flemming, H.-C. & Wuertz, S. Bacteria and archaea on Earth and their abundance in biofilms. *Nature Reviews Microbiology* **17**, 247-260 (2019).

Code Availability

All the codes and source data associated with the numerical simulations and analysis of this manuscript are available at the Github repository: (https://github.com/twang1993/MultistabilityByHGT).

Acknowledgements

This work is supported by Shenzhen Institute of Synthetic Biology Scientific Research Program (Grant No. HSE199011086). The funder had no role in study design, data collection and analysis, the decision to publish, or the preparation of the manuscript.

Declaration of interests

The authors declare no competing interests.